Supplement of

Towards harmonized measurements of condensable vapors: insights from the intercomparison of six chemical ionization mass spectrometers at a boreal forest site

Cecilia Righi et al.

Correspondence to: Cecilia Righi (cecilia.righi@helsinki.fi), Nina Sarnela (nina.sarnela@helsinki.fi)

S1 Abstract – description of the supporting material

This Supporting Information provides additional material to clarify and extend the analysis presented in the manuscript text, including supporting figures and tables. It is organized into Sections S1–S13: S1 Abstract – description of the supporting material, S2 ACTRIS CI-FI1 campaign timeline, S3 SmartSMEAR metadata, S4 Atmospheric Pressure interface Time-of-Flight mass spectrometer, S5 Peak lists, S6 Inlet tube losses, S7 Sulfuric acid calibration setup, S8 Equations used for the analysis of bromide mode data, S9 Considerations on the application of the transmission correction factor, S10 Measurements in nitrate mode – additional species, S11 Measurements in nitrate mode – correlation analysis, S12 Measurements in bromide mode – calibration factor, S13 Measurements in bromide mode – correlation analysis, S14 Measurements in different reagent ion modes: nitrate, bromide, and iodide – additional species, S15 References.

S2 ACTRIS CI-FI1 campaign timeline

Figure S1 shows a timeline of the ACTRIS CI-FI1 campaign.

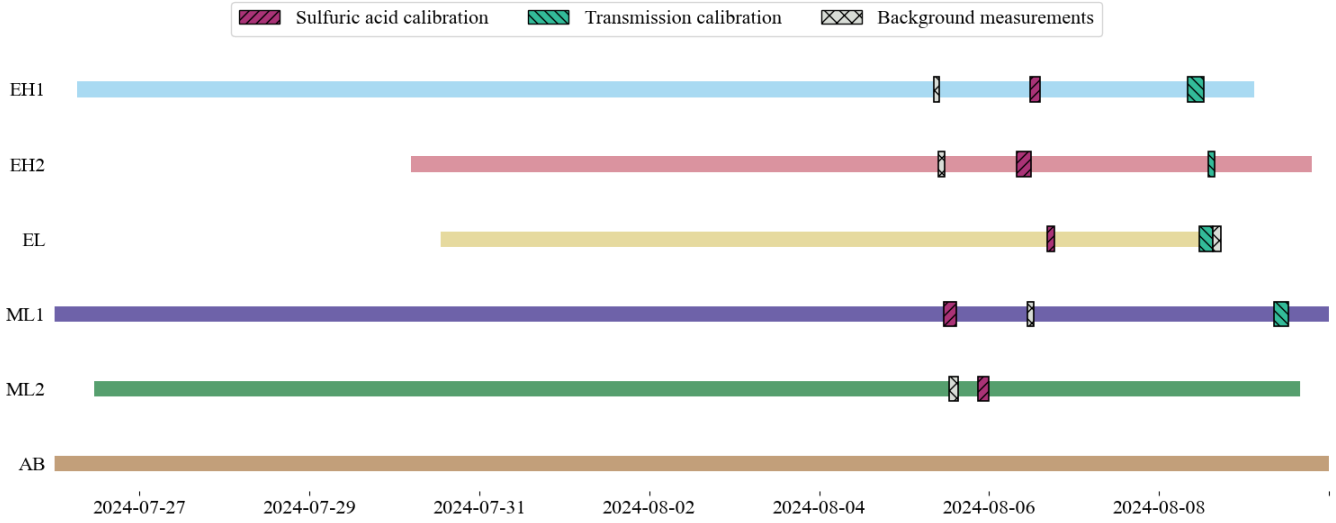

Figure S1 Schematic timeline of the ACTRIS CI-FI1 campaign. The horizontal bars indicate the time span during which each instrument was deployed, and are colored for better contrast. The figure highlights the timing of sulfuric acid calibrations (magenta), transmission calibrations (green), and background measurements (grey), performed during the campaign. Transmission calibration on ML2 was performed post-campaign in the ACTRIS Laboratory of the University of Helsinki.

S3 SmartSMEAR metadata

Table S1 provides metadata for the meteorological data retrieved from the SmartSMEAR database (https://smear.avaa.csc.fi/, last access: 13 January 2026) for the SMEAR II station during the measurement campaign period. These data were used to support the interpretation of the measurements from the instruments used in this study.

Table S1 Metadata of the meteorological variables retrieved from the SmartSMEAR database for the SMEAR II station during the campaign period.

title	Air temperature 16.8 m (2)	Relative humidity 16.8 m	Precipitation	UVB radiation
tableId	HYY_META	HYY_META	HYY_META	HYY_META
name	Tmm168	RH168	Precipacc	UV_B
description	Air temperature at 16.8 m height measured with Pt100 inside Rotronic RS12T/RS24T radiation shield, inconsistent with the old 4.2-67.2 m temperature profile	Relative humidity at 16.8 m height	Precipitation (liquid water equivalent) accumulated during previous 1 min	Ultraviolet B radiation in wavelength range 280-315 nm at 18 m height (radiation tower 1997-2/2017) or 35 m height (35 m tower 2/2017-), data until 2023 converted from erythemally weighted UVB to unweighted UVB with factor 7.55, high relative uncertainty at solar elevation angle of <20 degrees
unit	°C	%	mm	W m^{-2}
source	Pt100 inside Rotronic shield	Rotronic MP102H RH sensor, mastmet33	Vaisala FD12P weather sensor at 18 m height	Solar Light SL501A (-2023) or K&Z SUV-B (2024-)
periodStart	2013-01-22T00:00:00.0	2013-01-22T15:31:00.0	2005-04-01T00:00:00.0	1997-03-07T17:21:00.0
periodEnd	null	null	null	null
coverage	0	0	0	0
rights	public	public	public	public
mandatory	FALSE	FALSE	FALSE	FALSE
derivative	FALSE	FALSE	FALSE	FALSE
timestamp	2020-06-30T11:31:43	2020-12-22T13:33:07	2021-03-08T07:49:55	2024-10-04T12:41:42
category	Meteorology	Meteorology	Meteorology	Radiation

S4 Atmospheric Pressure interface Time-of-Flight mass spectrometer

The Atmospheric Pressure interface Time-of-Flight (APi-ToF) mass spectrometer is a high-resolution instrument capable of detecting ions sampled at atmospheric pressure (Junninen et al., 2010). Once the sampled ions enter the APi section through a 0.3 mm pinhole at a flow rate of ~0.8 L min^{-1}, neutral molecules are gradually pumped away, while the ions are focused at the center of the flow and guided from atmospheric pressure to the high vacuum of the ToF chamber (~10^{-6} mbar) via three differentially pumped stages. This gradual pressure drop helps prevent the loss of ions that could result from abrupt decompression. In the ToF chamber, ions are accelerated by a pulsed electric field, and their m/z are determined by measuring the time required to traverse a field-free region and reach the detector. Detection is performed using two microchannel plates (MCPs), each consisting of a dense array of microscopic channels that act as electron multipliers: when ions collide with the MCP surface, they generate an initial pulse of electrons, which then cascade through successive collisions along the channel walls, amplifying the signal. The resulting electron current is collected at the anode. Finally, data acquisition is carried out using either a time-to-digital converter, which records the arrival time of each ion exceeding a certain threshold, or an analog-to-digital converter, which continuously measures the ion signal intensity.

S5 Peak lists

This section presents the peak lists used for the comparison of the CI-APi-ToFs during the measurement campaign. Separate tables are provided for instruments operating in nitrate (NO_3^-), bromide (Br^-), and iodide (I^-) mode. In addition, tables listing the additional peaks included to account for the enhanced sensitivity of bromide toward less oxidized compounds are provided for both ionization modes. For convenience, nitrophenol is included within the group of strong organic and inorganic acids (HA), although it should be noted that it is not strictly a strong acid, given its relatively high pKa (~7.15). Nevertheless, nitrophenol can be efficiently detected in NO_3^- mode and is commonly regarded as a marker compound for biomass burning.

Table S2 Peak list selected for the instruments operating in nitrate (NO_3^-) mode. The monoisotopic mass (Th) corresponds to the exact mass of the detected ion. The last column indicates the species or chemical group assigned to each peak. In addition to highly oxygenated organic molecules (HOMs), semi-volatile organic compounds (SVOCs) were included to account for less oxidized organic compounds detectable in NO_3^- mode. The volatility of HOMs and SVOCs was estimated using the parametrization of Donahue et al. (2011), updated by Mohr et al. (2019), defined at reference temperature of 300 K.

Ion	Monoisotopic Mass (Th)	Volatility	Species / Group
NO_3^-	61.988		reagent ion
$(H_2O) \cdot NO_3^-$	79.999		reagent ion
$CH_3SO_3^-$	94.981		methanesulfonic acid / HA
HSO_4^-	96.960		sulfuric acid
$C_3H_3O_4^-$	103.004		malonic acid / HA
$(HNO_3) \cdot NO_3^-$	124.984		reagent ion

$C_6H_4NO_3^-$	138.020		nitrophenol / HA
$(CH_4SO_3) \cdot NO_3^-$	157.976		methanesulfonic acid / HA
$(HNO_3) \cdot HSO_4^-$	159.956		sulfuric acid
$(C_3H_4O_4) \cdot NO_3^-$	165.999		malonic acid / HA
IO_3^-	174.890		iodic acid / HA
$(HNO_3)_2 \cdot NO_3^-$	187.980		reagent ion
$(H_2SO_4) \cdot HSO_4^-$	194.927		sulfuric acid
$(C_6H_5NO_3) \cdot NO_3^-$	201.015		nitrophenol / HA
$(HIO_3) \cdot NO_3^-$	237.885		iodic acid / HA
$(C_{10}H_{14}O_3) \cdot NO_3^-$	244.083	SVOC	closed shell non-nitrate monomers / SVOC
$(C_{10}H_{16}O_3) \cdot NO_3^-$	246.098	SVOC	closed shell non-nitrate monomers / SVOC
$(C_{10}H_{14}O_4) \cdot NO_3^-$	260.078	SVOC	closed shell non-nitrate monomers / SVOC
$(C_{10}H_{15}O_4) \cdot NO_3^-$	261.085	SVOC	organic peroxy radicals / SVOC
$(C_{10}H_{16}O_4) \cdot NO_3^-$	262.093	SVOC	closed shell non-nitrate monomers / SVOC
$(C_{10}H_{16}O_5) \cdot NO_3^-$	278.088	SVOC	closed shell non-nitrate monomers / SVOC
$(C_{10}H_{14}O_6) \cdot NO_3^-$	292.067	SVOC	closed shell non-nitrate monomers / SVOC
$(H_2SO_4)_2 \cdot HSO_4^-$	292.895		sulfuric acid
$(C_{10}H_{15}O_6) \cdot NO_3^-$	293.075	SVOC	organic peroxy radicals / SVOC
$(C_{10}H_{16}O_6) \cdot NO_3^-$	294.083	SVOC	closed shell non-nitrate monomers / SVOC
$(C_{10}H_{14}O_7) \cdot NO_3^-$	308.062	LVOC	closed shell non-nitrate monomers / HOM
$(C_{10}H_{16}O_7) \cdot NO_3^-$	310.078	LVOC	closed shell non-nitrate monomers / HOM
$(C_{10}H_{14}O_8) \cdot NO_3^-$	324.057	LVOC	closed shell non-nitrate monomers / HOM
$(C_{10}H_{15}O_8) \cdot NO_3^-$	325.065	LVOC	organic peroxy radicals / HOM
$(C_{10}H_{16}O_8) \cdot NO_3^-$	326.073	LVOC	closed shell non-nitrate monomers / HOM
$(C_{10}H_{15}O_8N) \cdot NO_3^-$	339.068	LVOC	closed shell organonitrate monomers / HOM
$(C_{10}H_{14}O_9) \cdot NO_3^-$	340.052	LVOC	closed shell non-nitrate monomers / HOM
$(C_{10}H_{16}O_9) \cdot NO_3^-$	342.068	LVOC	closed shell non-nitrate monomers / HOM
$(C_{10}H_{15}O_9N) \cdot NO_3^-$	355.063	LVOC	closed shell organonitrate monomers / HOM
$(C_{10}H_{14}O_{10}) \cdot NO_3^-$	356.047	LVOC	closed shell non-nitrate monomers / HOM

$(C_{10}H_{15}O_{10}) \cdot NO_3^-$	357.055	LVOC	organic peroxy radicals / HOM
$(C_{10}H_{16}O_{10}) \cdot NO_3^-$	358.063	LVOC	closed shell non-nitrate monomers / HOM
$(C_{10}H_{14}O_{11}) \cdot NO_3^-$	372.042	LVOC	closed shell non-nitrate monomers / HOM
$(C_{10}H_{16}O_{11}) \cdot NO_3^-$	374.058	LVOC	closed shell non-nitrate monomers / HOM
$(C_{10}H_{15}O_{11}N) \cdot NO_3^-$	387.053	LVOC	closed shell organonitrate monomers / HOM
$(C_{19}H_{28}O_{11}) \cdot NO_3^-$	494.152	ULVOC	dimers / HOM
$(C_{19}H_{28}O_{12}) \cdot NO_3^-$	510.146	ULVOC	dimers / HOM
$(C_{20}H_{30}O_{12}) \cdot NO_3^-$	524.162	ULVOC	dimers / HOM
$(C_{20}H_{32}O_{13}) \cdot NO_3^-$	542.173	ULVOC	dimers / HOM
$(C_{20}H_{31}O_{13}N) \cdot NO_3^-$	555.168	ULVOC	nitrate dimers / HOM
$(C_{20}H_{30}O_{14}) \cdot NO_3^-$	556.152	ULVOC	dimers / HOM
$(C_{20}H_{32}O_{15}) \cdot NO_3^-$	574.162	ULVOC	dimers / HOM
$(C_{20}H_{30}O_{16}) \cdot NO_3^-$	588.142	ULVOC	dimers / HOM
$(C_{20}H_{30}O_{18}) \cdot NO_3^-$	620.132	ULVOC	dimers / HOM

Table S3 Peak list selected for the instruments operating in bromide (Br^-) mode. The monoisotopic mass (Th) corresponds to the exact mass of the detected ion. The last column indicates the species or chemical group assigned to each peak. In addition to highly oxygenated organic molecules (HOMs), semi-volatile organic compounds (SVOCs) were included to account for less oxidized organic compounds detectable in NO_3^- mode. The volatility of HOMs and SVOCs was estimated using the parametrization of Donahue et al. (2011), updated by Mohr et al. (2019), defined at reference temperature of 300 K.

Ion	Monoisotopic Mass (Th)	Volatility	Species / Group
Br^-	78.919		reagent ion
$CH_3SO_3^-$	94.981		methanesulfonic acid / HA
$(H_2O) \cdot Br^-$	96.929		reagent ion
HSO_4^-	96.960		sulfuric acid
$C_3H_3O_4^-$	103.004		malonic acid / HA
$C_6H_4NO_3^-$	138.020		nitrophenol / HA
IO_3^-	174.890		iodic acid / HA
$(CH_4SO_3) \cdot Br^-$	174.907		methanesulfonic acid / HA
$(H_2SO_4) \cdot Br^-$	176.886		sulfuric acid
$(C_3H_4O_4) \cdot Br^-$	182.930		malonic acid / HA

$(C_6H_5NO_3) \cdot Br^-$	217.946		nitrophenol / HA
$(HIO_3) \cdot Br^-$	254.816		iodic acid / HA
$(C_{10}H_{14}O_3) \cdot Br^-$	261.013	SVOC	closed shell non-nitrate monomers / SVOC
$(C_{10}H_{16}O_3) \cdot Br^-$	263.029	SVOC	closed shell non-nitrate monomers / SVOC
$(C_{10}H_{14}O_4) \cdot Br^-$	277.008	SVOC	closed shell non-nitrate monomers / SVOC
$(C_{10}H_{15}O_4) \cdot Br^-$	278.016	SVOC	organic peroxy radicals / SVOC
$(C_{10}H_{16}O_4) \cdot Br^-$	279.024	SVOC	closed shell non-nitrate monomers / SVOC
$(C_{10}H_{16}O_5) \cdot Br^-$	295.019	SVOC	closed shell non-nitrate monomers / SVOC
$(C_{10}H_{14}O_6) \cdot Br^-$	308.998	SVOC	closed shell non-nitrate monomers / SVOC
$(C_{10}H_{15}O_6) \cdot Br^-$	310.006	SVOC	organic peroxy radicals / SVOC
$(C_{10}H_{16}O_6) \cdot Br^-$	311.014	SVOC	closed shell non-nitrate monomers / SVOC
$(C_{10}H_{14}O_7) \cdot Br^-$	324.993	LVOC	closed shell non-nitrate monomers / HOM
$(C_{10}H_{16}O_7) \cdot Br^-$	327.008	LVOC	closed shell non-nitrate monomers / HOM
$(C_{10}H_{14}O_8) \cdot Br^-$	340.988	LVOC	closed shell non-nitrate monomers / HOM
$(C_{10}H_{15}O_8) \cdot Br^-$	341.996	LVOC	organic peroxy radicals / HOM
$(C_{10}H_{16}O_8) \cdot Br^-$	343.003	LVOC	closed shell non-nitrate monomers / HOM
$(C_{10}H_{15}O_8N) \cdot Br^-$	355.999	LVOC	closed shell organonitrate monomers / HOM
$(C_{10}H_{14}O_9) \cdot Br^-$	356.983	LVOC	closed shell non-nitrate monomers / HOM
$(C_{10}H_{16}O_9) \cdot Br^-$	358.998	LVOC	closed shell non-nitrate monomers / HOM
$(C_{10}H_{15}O_9N) \cdot Br^-$	371.994	LVOC	closed shell organonitrate monomers / HOM
$(C_{10}H_{14}O_{10}) \cdot Br^-$	372.978	LVOC	closed shell non-nitrate monomers / HOM
$(C_{10}H_{15}O_{10}) \cdot Br^-$	373.985	LVOC	organic peroxy radicals / HOM
$(C_{10}H_{16}O_{10}) \cdot Br^-$	374.993	LVOC	closed shell non-nitrate monomers / HOM
$(C_{10}H_{14}O_{11}) \cdot Br^-$	388.972	LVOC	closed shell non-nitrate monomers / HOM
$(C_{10}H_{16}O_{11}) \cdot Br^-$	390.988	LVOC	closed shell non-nitrate monomers / HOM
$(C_{10}H_{15}O_{11}N) \cdot Br^-$	403.983	LVOC	closed shell organonitrate monomers / HOM
$(C_{19}H_{28}O_{11}) \cdot Br^-$	511.082	ULVOC	dimers / HOM
$(C_{19}H_{28}O_{12}) \cdot Br^-$	527.077	ULVOC	dimers / HOM
$(C_{20}H_{30}O_{12}) \cdot Br^-$	541.093	ULVOC	dimers / HOM

$(C_{20}H_{32}O_{13}) \cdot Br^-$	559.103	ULVOC	dimers / HOM
$(C_{20}H_{31}O_{13}N) \cdot Br^-$	572.098	ULVOC	nitrate dimers / HOM
$(C_{20}H_{30}O_{14}) \cdot Br^-$	573.082	ULVOC	dimers / HOM
$(C_{20}H_{32}O_{15}) \cdot Br^-$	591.093	ULVOC	dimers / HOM
$(C_{20}H_{30}O_{16}) \cdot Br^-$	605.072	ULVOC	dimers / HOM
$(C_{20}H_{30}O_{18}) \cdot Br^-$	637.062	ULVOC	dimers / HOM

Table S4 Peak list selected for the instruments operating in iodide (I^-) mode. The monoisotopic mass (Th) corresponds to the exact mass of the detected ion. The last column indicates the species or chemical group assigned to each peak. The volatility of the organic compounds was estimated using the parametrization of Donahue et al. (2011), updated by Mohr et al. (2019), defined at reference temperature of 300 K.

Ion	Monoisotopic Mass (Th)	Volatility	Species / Group
$(C_{10}H_{14}O_3) \cdot I^-$	308.999	SVOC	closed shell non-nitrate monomers / SVOC
$(C_{10}H_{16}O_3) \cdot I^-$	311.015	SVOC	closed shell non-nitrate monomers / SVOC
$(C_{10}H_{14}O_4) \cdot I^-$	324.994	SVOC	closed shell non-nitrate monomers / SVOC
$(C_{10}H_{16}O_4) \cdot I^-$	327.010	SVOC	closed shell non-nitrate monomers / SVOC
$(C_{10}H_{16}O_5) \cdot I^-$	343.005	SVOC	closed shell non-nitrate monomers / SVOC
$(C_{10}H_{14}O_6) \cdot I^-$	356.984	SVOC	closed shell non-nitrate monomers / SVOC

S6 Inlet tube losses

Sulfuric acid wall losses are already accounted for in the model used to calculate sulfuric acid concentrations in the calibration experiment (Kürten et al., 2012); therefore, no additional correction factor is required when deriving concentrations from ion count rates. For species other than sulfuric acid, however, a factor C_{inlet} was introduced to account for losses in the inlet tube, calculated following the steps outlined below.

1. A gas diffusion coefficient, D_g (cm^2 s^{-1}), is calculated for each compound as:

$$D_{AB} = \frac{1\times10^{-3}\cdot T^{1.75}\cdot\sqrt{\frac{1}{M_A}+\frac{1}{M_B}}}{p\cdot\left(\sqrt[3]{\sum_A v_i}+\sqrt[3]{\sum_B v_i}\right)^2}, \quad \text{Eq. (S1)}$$

where T (K) is the temperature, p (atm) is the pressure, $M_{A,B}$ (g mol^{-1}) are the molecular mass of air (A) and the species of interest (B), v_i (cm^{-3}) is the atomic diffusion volume to be summed over the atoms/groups of each diffusing species. v_i values have been derived from Fuller et al. (1969).

2. The frequency of wall collision, k (s^{-1}) is calculated for each species using the following equation, assuming a first-order loss process:

$$k = 3.6 \cdot \frac{D_{AB}}{r_{in}^2}, \quad \text{Eq. (S2)}$$

where r_{in} (cm) is the radius of the inlet tube.

3. The residence time of the gas inside the inlet tube, Rt_{in} (s), is calculated as:

$$Rt_{in} = \frac{\pi \cdot r_{in}^2 \cdot l_{in}}{\frac{Q_{in}}{60} \cdot 10^3}, \quad \text{Eq. (S3)}$$

where l_{in} (cm) and Q_{in} (L min^{-1}) are the inlet tube length and flow rate, respectively.

4. The inlet tube loss is calculated for each species as:

$$L_{in} = 1 - e^{-k * Rt_{in}}. \quad \text{Eq. (S4)}$$

5. Finally, the loss correction factor is calculated as:

$$C_{inlet} = \frac{1}{1 - L_{in}}. \quad \text{Eq. (S5)}$$

S7 Sulfuric acid calibration setup

The calibration setup (Figure S2) was built based on the one presented by Kürten et al. (2012), with a few key differences. First, the dimensions of the box in our setup are 14 × 14 × 8 cm (L × W × H), with a 3/4"-diameter tube passing through the box, whereas Kürten et al. (2012) used a box of 30 × 20 × 15 cm and a 1/2"-diameter tube. Second, our setup does not include a photodiode for monitoring lamp stability.

The aluminum box houses a Pen-Ray® Hg Lamp (Analytik Jena US LLC), which serves as the UV source responsible for the photolysis of H_2O vapor and the in-situ production of H_2SO_4 via the following reactions:

$$OH + SO_2 + M \rightarrow HSO_3 + M \quad \text{(R1)}$$

$$HSO_3 + O_2 \rightarrow SO_3 + HO_2 \quad \text{(R2)}$$

$$SO_3 + 2H_2O \rightarrow H_2SO_4 + H_2O \quad \text{(R3)}$$

Four mass flow controllers (MFCs; Alicat Scientific MC-series) were used to regulate the inflow rates of sulfur dioxide, synthetic air, and nitrogen. The nitrogen flow was first split into three separate lines: (1) a carrier gas line, (2) a line for H_2O vapor production, and (3) a line for flushing the Hg lamp. The carrier gas and H_2O vapor lines were each regulated by a MFC, while the Hg-lamp flush was adjusted using a needle valve. To generate water vapor, the N_2 flow from the second MFC passed through a bottle containing Milli-Q H_2O, which served as a humidifier. All tubing was made of Teflon® with a diameter of 6 mm, except for the 3/4"-diameter stainless steel tube passing through the box.

When connecting the calibration setup to the CI-APi-ToF, the nitrogen flush to the aluminum box was set to 1.5 L min^{-1}, and the lamp was switched on and allowed to warm up for approximately 90 min. After this period, the gas flow rates were adjusted via the MFCs so that their sum slightly exceeded the flow drawn into the inlet. Each calibration step lasted 10

minutes, after which the incoming wet nitrogen flow was modified while keeping the other parameters constant. The calibration experiment consisted of five steps, repeated twice.

Following Kürten et al. (2012), chemical actinometry was used to estimate the It-product needed for modeling H_2SO_4 concentrations. For this study, the actinometry experiment was conducted in January 2024 at the ACTRIS Laboratory of the University of Helsinki. Further instructions and best practices for sulfuric acid calibration and actinometry experiment are available on GitHub at https://github.com/ceciliarighi/ACTRIS_CiGas_condensable_vapors.

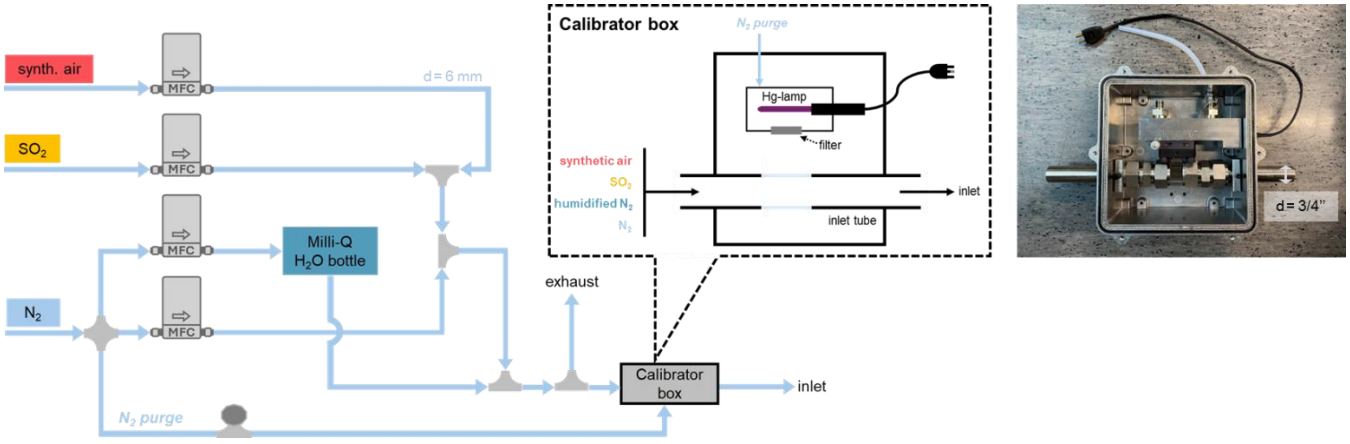

Figure S2 Schematic diagram of the calibration setup used for the sulfuric acid calibration during the measurement campaign.

S8 Equations used for the analysis of bromide mode data

Here we report the equations used to calculate the concentrations of sulfuric acid, acidic organic and inorganic compounds (HAs), and highly oxygenated organic molecules (HOMs) from bromide mode measurements. Equations (S6)–(S8) are analogous to Eqs. (2)–(4) presented in the main text for nitrate mode data. In addition, Eq. (S9) describes the calculation of concentrations for the semi-volatile organic compounds (SVOCs) group.

$$[H_2SO_4] = \frac{HSO_4^- + H_2SO_4 \cdot Br^-}{Br^- + H_2O \cdot Br^-} \times C'_{SA} \,, \qquad \text{Eq. (S6)}$$

$$[HA] = \frac{A^- + HA \cdot Br^-}{Br^- + H_2O \cdot Br^-} \times C'_{SA} \times C_{inlet} \,, \qquad \text{Eq. (S7)}$$

$$[HOM] = \frac{HOM \cdot Br^-}{Br^- + H_2O \cdot Br^-} \times C'_{SA} \times C_{inlet} \times C_{trans} \,, \qquad \text{Eq. (S8)}$$

$$[SVOC] = \frac{HOM \cdot Br^-}{Br^- + H_2O \cdot Br^-} \times C'_{SA} \times C_{inlet} \times C_{trans} \,. \qquad \text{Eq. (S9)}$$

As discussed in Sect. 2.2.5, Br^- ionization is not fully kinetically limited for HOMs, implying lower charging efficiency than for sulfuric acid and HAs compared to NO_3^-, which in turn exhibits lower sensitivity toward the less oxygenated SVOCs.

Equation (S10) is analogous to Eq. (1) in the manuscript text and was used to calculate the sulfuric acid signal normalized to the reagent ion signal during the sulfuric acid calibration experiments.

$$S_{H_2SO_4} = \frac{HSO_4^- + H_2SO_4 \cdot Br^-}{Br^- + H_2O \cdot Br^-} . \quad \text{Eq. (S10)}$$

S9 Considerations on the application of the transmission correction factor

Figure S3 **Figure S3** visually supports the considerations discussed in Sect. 3.2 of the manuscript text, highlighting the effect of applying different correction factors to the data measured by the five CI-APi-ToFs operating in nitrate mode.

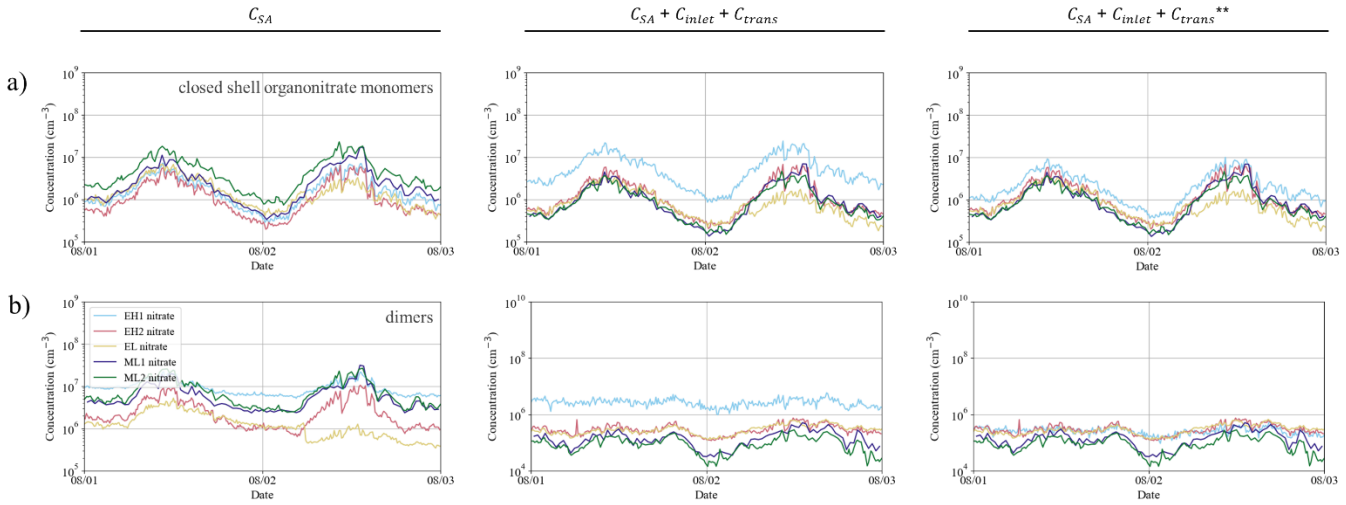

Figure S3 Concentrations of (a) closed shell organonitrate monomers, and (b) dimers measured in nitrate mode by five mass spectrometers during 1-2 August 2024. For each panel, the left plot shows concentration time series obtained by applying only the sulfuric acid calibration factor (C_{SA}); the central plot shows concentrations obtained by applying C_{SA}, inlet loss correction (C_{inlet}), and transmission correction (C_{trans}) to all instruments; right plot shows concentrations obtained by applying C_{SA}, C_{inlet}, and C_{trans} to all instruments except EH1.

Table S5, analogous to Table 5 for nitrate mode, show the results of the correlation analysis performed on concentrations of different HOM classes measured by ML1 and ML2 operating in Br^- modes on 27–31 July 2024.

Table S5 Coefficients of determination (R^2) and relative median absolute deviation (rMAD) calculated from concentrations of different HOM classes measured by ML1 and ML2 on 27–31 July 2024. Values are shown for cases (a) where only C'_{SA} is applied, and (b) where C'_{SA}, C_{inlet}, and C_{trans} are applied.

HOM class	R_a^2	R_b^2	$rMAD_a$ [%]	$rMAD_b$ [%]
organic peroxy radicals	0.826	0.828	56.5	30.1
closed shell non-nitrate monomers	0.785	0.782	25.4	14.3
closed shell organonitrate monomers	0.730	0.725	27.2	39.4

dimers	0.132	0.131	94.4	88.5
semi-volatile organic compounds	0.877	0.853	22.3	6.1

S10 Measurements in nitrate mode – additional species

Figure S4 shows time series and box plots for additional HOM classes measured in nitrate mode on 1–2 August 2024, complementing Figure 5 of the manuscript text.

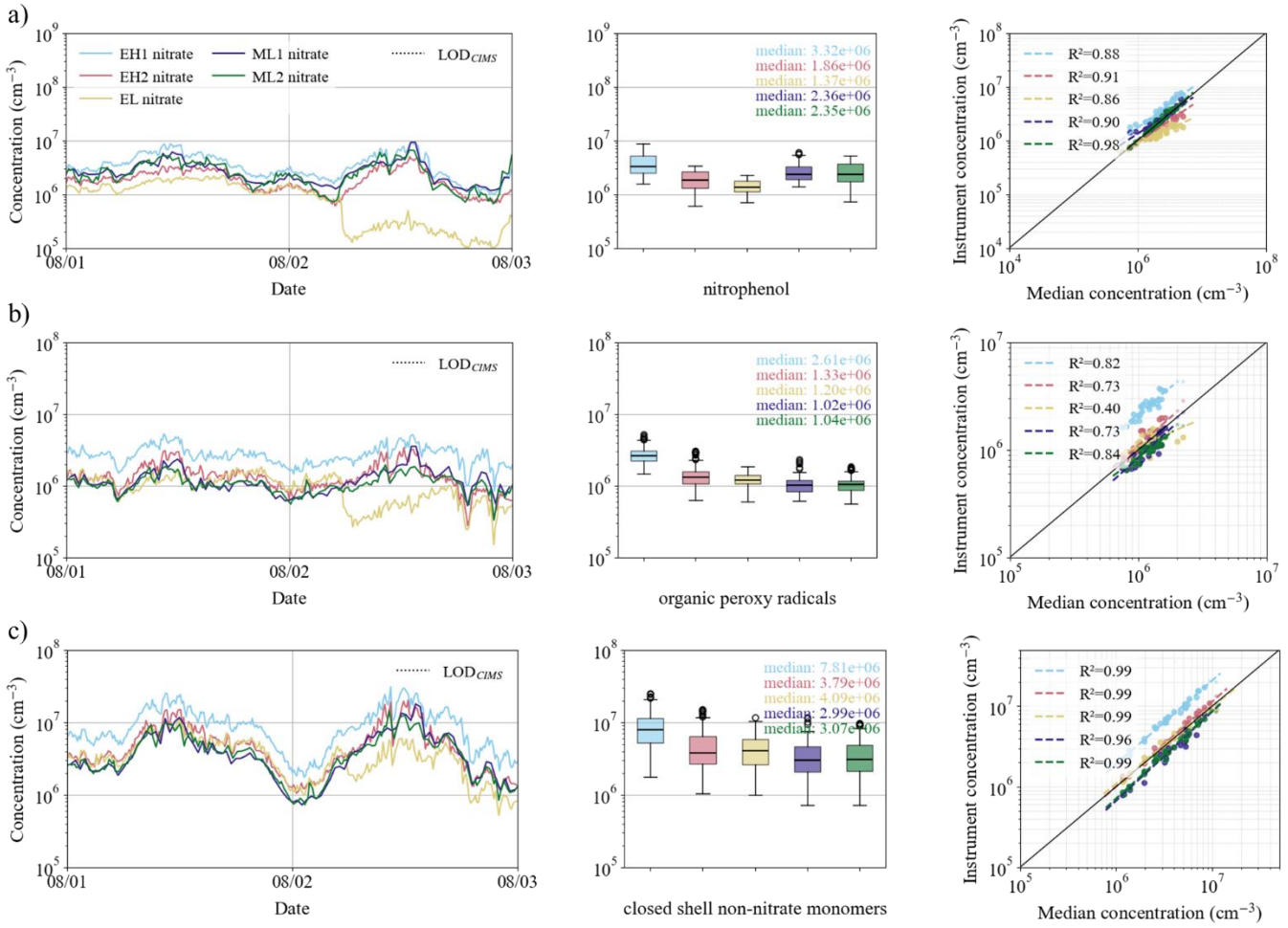

Figure S4 Concentrations of (a) nitrophenol, (b) organic peroxy radicals, and (c) closed-shell non-nitrate monomers measured in nitrate mode by five mass spectrometers during 1-2 August 2024. For each panel, the left plot shows concentration time series, with instrument-specific LOD values indicated by dotted horizontal lines. The central plot shows a box plot summarizing the distributions over the same period; boxes indicate the interquartile range, horizontal lines indicate the median, whiskers represent the non-outlier range, and empty circles denote outliers. Data points below LOD are excluded from the box plot. The right plot shows hourly median concentrations measured by each instrument against the hourly median concentration across all five instruments. Dashed lines indicate log–log linear regressions for each instrument, with the corresponding coefficient of determination (R^2) reported in the legend. Points below the corresponding LOD are shown as crosses (X), while outliers are plotted as smaller semi-transparent points. The abrupt shift in the EL time

series occurring around 05:40 on 2 August was caused by an issue encountered while adjusting the nitric acid flow mixed with the sheath flow.

S11 Measurements in nitrate mode – correlation analysis

Table S6-Table S7, analogous to Table 6 in the manuscript text, report the results of the correlation analysis for the species targeted in NO_3^- mode based on data recorded by the five CI-APi-ToFs. In Table S6, concentrations were calculated by applying only C_{SA} to all species. In Table S7 and Table S8, concentrations were calculated by applying C_{SA}, C_{inlet} and C_{trans}; however, in the latter, data from EH1 were excluded from the correlation analysis to assess whether some of the low R^2 values could be attributed to the different behavior of this instrument in specific m/z ranges.

Table S6 Statistical parameters of the correlation analysis for the species measured in nitrate mode based on data recorded by the five CI-APi-ToFs. R^2 is the coefficient of determination, p is the probability value, and parameters a and b are the slope and the offset of the linear fit, respectively. Concentrations were calculated by applying only C_{SA} to all species.

Species	R^2	p	a	b
sulfuric acid	0.577	<0.001	0.897	0.525
methanesulfonic acid	0.271	<0.001	0.677	1.579
malonic acid	0.561	<0.001	0.995	0.010
iodic acid	0.339	<0.001	0.959	0.140
nitrophenol	0.314	<0.001	0.666	2.068
organic peroxy radicals	0.037	<0.05	0.394	3.859
closed shell non-nitrate monomers	0.625	<0.001	0.951	0.343
closed shell organonitrate monomers	0.730	<0.001	0.963	0.248
dimers	0.288	<0.001	0.653	1.907

Table S7 Statistical parameters of the correlation analysis for the species measured in nitrate mode based on data recorded by the five CI-APi-ToFs. R^2 is the coefficient of determination, p is the probability value, and parameters a and b are the slope and the offset of the linear fit, respectively. Concentrations were calculated by applying C_{SA}, C_{inlet}, and C_{trans} to all species.

Species	R^2	p	a	b
sulfuric acid	0.577	<0.001	0.897	0.525
methanesulfonic acid	0.110	<0.001	0.587	2.188
malonic acid	0.450	<0.001	0.923	0.549
iodic acid	0.088	<0.001	0.599	1.815
nitrophenol	0.433	<0.001	0.815	1.185

organic peroxy radicals	0.012	>0.05	0.303	4.349
closed shell non-nitrate monomers	0.415	<0.001	0.917	0.644
closed shell organonitrate monomers	0.555	<0.001	0.956	0.369
dimers	0.003	>0.05	-0.186	6.395

Table S8 Statistical parameters of the correlation analysis for the species measured in nitrate mode based on data recorded by four CI-APi-ToFs; EH1 data were excluded from the analysis. R^2 is the coefficient of determination, p is the probability value, and parameters a and b are the slope and the offset of the linear fit, respectively. Concentrations were calculated by applying C_{SA}, C_{inlet}, and C_{trans} to all species.

Species	R^2	p	a	b
sulfuric acid	0.379	<0.001	0.711	1.514
methanesulfonic acid	0.063	<0.05	0.487	2.728
malonic acid	0.291	<0.001	0.755	1.723
iodic acid	0.022	>0.05	0.189	3.627
nitrophenol	0.681	<0.001	0.829	1.057
organic peroxy radicals	0.320	<0.001	0.637	2.205
closed shell non-nitrate monomers	0.831	<0.001	0.934	0.435
closed shell organonitrate monomers	0.891	<0.001	0.965	0.207
dimers	0.004	>0.05	-0.073	5.539

S12 Measurements in bromide mode – calibration factor

Figure S5 reproduces the analysis presented in Figure 6 in the manuscript text, but with ML1 concentrations calculated using the sulfuric acid calibration factor derived during the campaign, C_{SA}, instead of the revised C'_{SA}. We decided to disregard this factor (1) because this calibration did not agree with the others performed on the same instrument, and (2) due to the behavior observed in Figure S5a. Specifically, ML1 and Ml2 show a nearly identical response to temporal variations in SVOC concentrations, while their absolute concentrations are offset by an approximately constant factor. This systematic shift is particularly evident in the scatter plot, where the two datasets align closely but are displaced relative to one another.

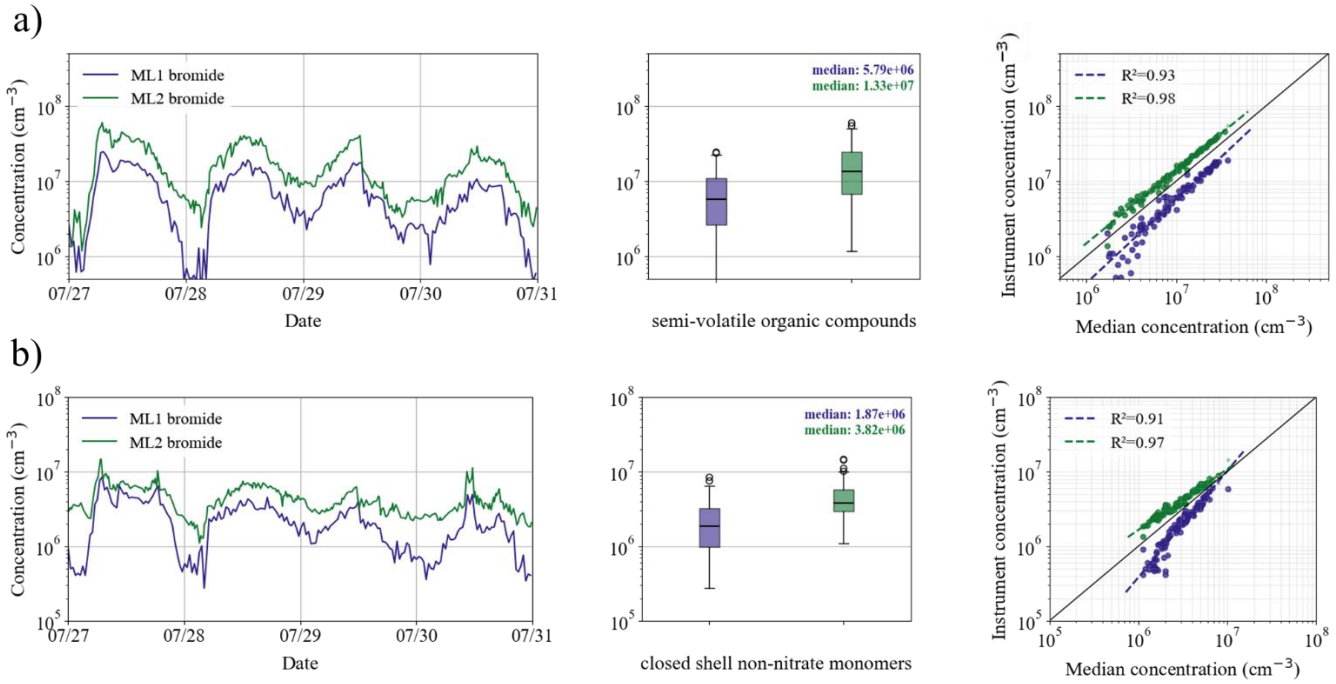

Figure S5 Concentrations of (a) semi-volatile organic compounds, and (b) closed-shell non-nitrate monomers measured in bromide mode by two mass spectrometers during 27-30 July 2024. For each panel, the left plot shows concentration time series, while the central plot shows box plots summarizing the distributions over the same period. Boxes indicate the interquartile range, horizontal lines indicate the median, whiskers represent the non-outlier range, and empty circles denote outliers. The right plot shows hourly median concentrations measured by each instrument against the hourly mean concentration across the two instruments. Dashed lines indicate log–log linear regressions for each instrument, with the corresponding coefficient of determination (R^2) reported in the legend. Outliers are plotted as smaller semi-transparent points. The concentrations have been calculated using the original C_{SA} derived for ML1 during the campaign, in place of the revised C'_{SA}, as it is for Figure 6 in the manuscript text.

S13 Measurements in bromide mode – correlation analysis

Table S9 and Table S10 report the results of the correlation analysis for the species targeted in Br^- mode based on data recorded by ML1 and ML2. In Table S9, concentrations were calculated by applying only C_{SA} (or C'_{SA}) to all species. In Table S10, concentrations were calculated by applying C_{SA} (or C'_{SA}), C_{inlet}, and C_{trans}.

Table S9 Statistical parameters of the correlation analysis for the species measured in bromide mode based on data recorded by ML1 and ML2. R^2 is the coefficient of determination, p is the probability value, and parameters a and b are the slope and the offset of the linear fit, respectively. Concentrations were calculated by applying only C_{SA} (or C'_{SA}) to all species.

Species	R^2	p	a	b
sulfuric acid	0.557	<0.001	0.812	1.201
closed shell non-nitrate monomers	0.785	<0.001	0.495	3.807
closed shell organonitrate monomers	0.730	<0.001	0.277	4.615

semi-volatile organic compounds	0.853	<0.001	0.785	1.811

Table S10 Statistical parameters of the correlation analysis for the species measured in bromide mode based on data recorded by ML1 and ML2. R^2 is the coefficient of determination, p is the probability value, and parameters a and b are the slope and the offset of the linear fit, respectively. Concentrations were calculated by applying C_{SA} (or C'_{SA}), C_{inlet}, and C_{trans} to all species.

Species	R^2	p	a	b
sulfuric acid	0.557	<0.001	0.812	1.201
closed shell non-nitrate monomers	0.782	<0.001	0.501	3.282
closed shell organonitrate monomers	0.725	<0.001	0.273	4.023
semi-volatile organic compounds	0.853	<0.001	0.783	1.554

S14 Measurements in different reagent ion modes: nitrate, bromide, and iodide – additional species

Figure S6 and Figure S7 extend the analysis shown in Figure 8 in the manuscript text to additional compounds.

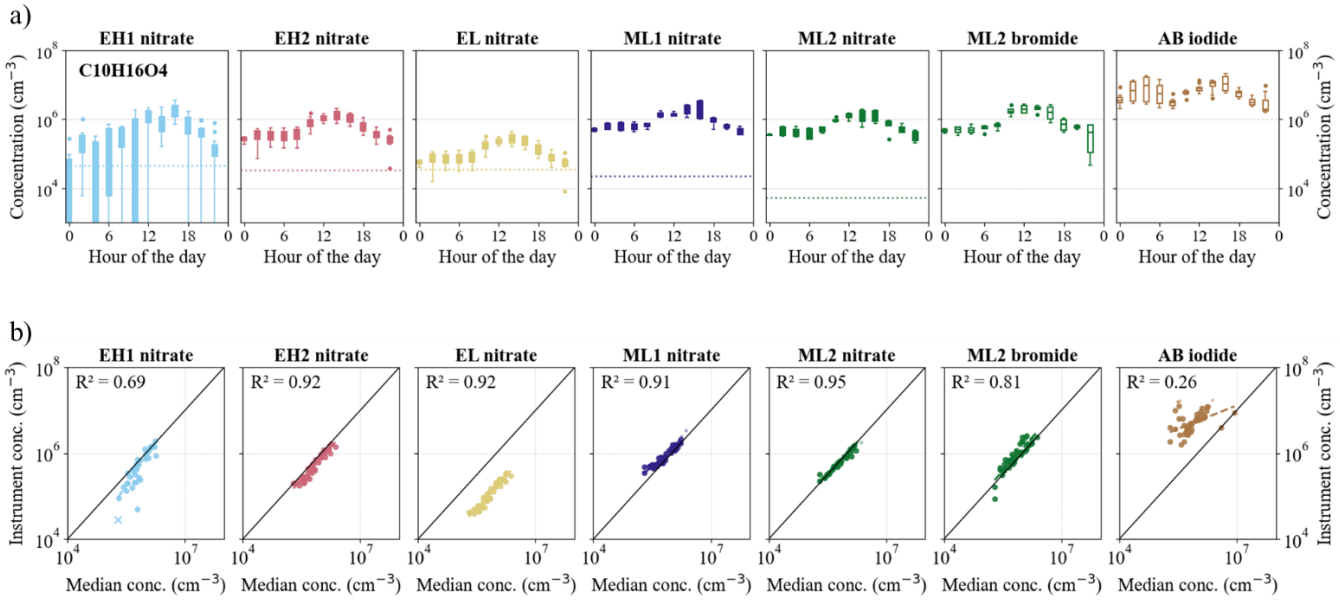

Figure S6 (a) Box plots showing the diurnal variation of $C_{10}H_{16}O_4$ based on measurements conducted on 1-2 August 2024. Data are from five instruments operating in nitrate mode (EH1, EH2, EL, ML1, ML2), one instrument operating in bromide mode (ML2), and one instrument operating in iodide mode (AB). Boxes indicate the interquartile range, whiskers represent the non-outlier range, and full circles denote outliers. (b) Scatter plots of hourly median concentrations showing, for each instrument and ionization mode combination, the concentrations measured by the individual instrument-mode against the median concentration measured across all instruments-mode combinations over the same period. Dashed lines indicate linear regressions for each instrument, with the corresponding coefficient of determination (R^2) reported in the figure.

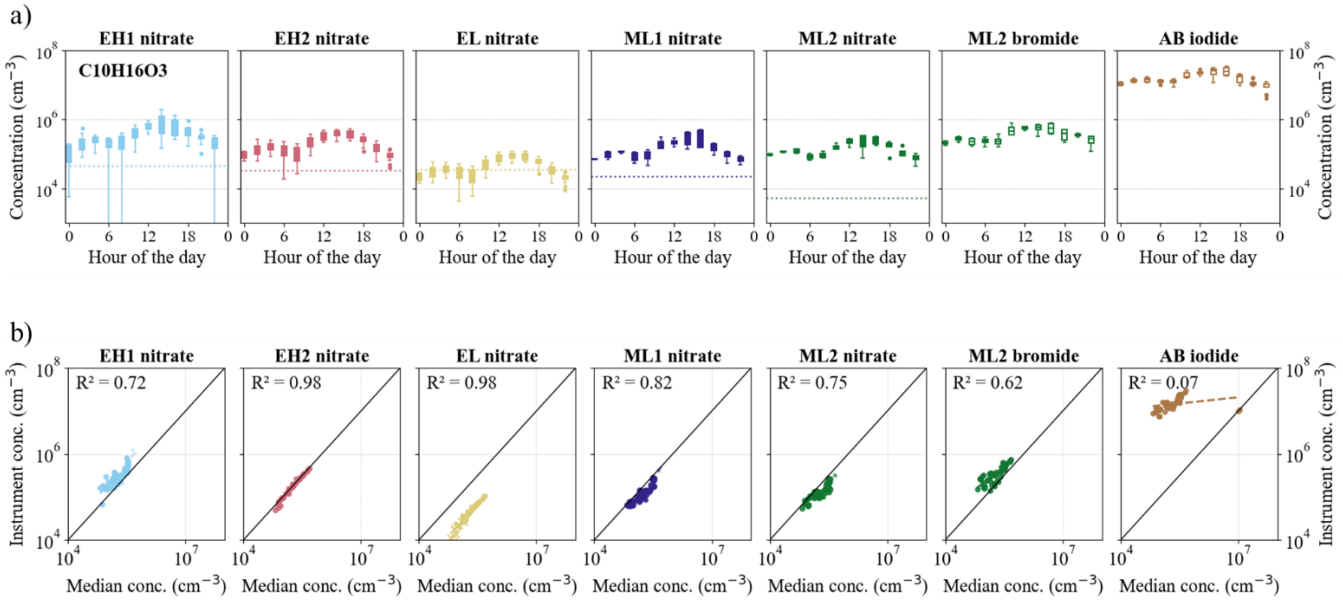

Figure S7 (a) Box plots showing the diurnal variation of $C_{10}H_{16}O_3$ based on measurements conducted on 1-2 August 2024. Data are from five instruments operating in nitrate mode (EH1, EH2, EL, ML1, ML2), one instrument operating in bromide mode (ML2), and one instrument operating in iodide mode (AB). Boxes indicate the interquartile range, whiskers represent the non-outlier range, and full circles denote outliers. (b) Scatter plots of hourly median concentrations showing, for each instrument and ionization mode combination, the concentrations measured by the individual instrument-mode against the median concentration measured across all instruments-mode combinations over the same period. Dashed lines indicate linear regressions for each instrument, with the corresponding coefficient of determination (R^2) reported in the figure.

S15 References

Donahue, N. M., Epstein, S. A., Pandis, S. N., and Robinson, A. L.: A two-dimensional volatility basis set: 1. organic-aerosol mixing thermodynamics, Atmos. Chem. Phys., 11, 3303–3318, https://doi.org/10.5194/acp-11-3303-2011, 2011.

Fuller, E. N., Ensley, K., and Giddings, C. J.: Diffusion of Halogenated Hydrocarbons in Helium. The Effect of Structure on Collision Cross Sections, J. Phys. Chem., 73, 3679–3685, https://doi.org/10.1021/j100845a020, 1969.

Junninen, H., Ehn, M., Petäjä, Luosujärvi, L., Kotiaho, T., Kostiainen, R., Rohner, U., Gonin, M., Fuhrer, K., Kulmala, M., and Worsnop, D. R.: A high-resolution mass spectrometer to measure atmospheric ion composition, Atmos. Meas. Tech., 3, 1039–1053, https://doi.org/10.5194/amt-3-1039-2010, 2010.

Kürten, A., Rondo, L., Ehrhart, S., and Curtius, J.: Calibration of a chemical ionization mass spectrometer for the measurement of gaseous sulfuric acid, Journal of Physical Chemistry A, 116, 6375–6386, https://doi.org/10.1021/jp212123n, 2012.

Mohr, C., Thornton, J. A., Heitto, A., Lopez-Hilfiker, F. D., Lutz, A., Riipinen, I., Hong, J., Donahue, N. M., Hallquist, M., Petäjä, T., Kulmala, M., and Yli-Juuti, T.: Molecular identification of organic vapors driving atmospheric nanoparticle growth, Nat. Commun., 10, https://doi.org/10.1038/s41467-019-12473-2, 2019.

235